Bol. Soc. Paran. Mat.
©SPM – E-ISSN-2175-1188
SPM: www.spm.uem.br/bspm

(3s.) **v. 2026 (44) 15** : 1–15.
ISSN-0037-8712
doi:10.5269/bspm.81681

MHD Mixed Convection Flow of a Hybrid Nanofluid over an Inclined Plate in a Porous Medium Using the Reduced Differential Transform Method

Konduru Sarada, J. Komathi, N. Magesh, P. Siva Kota Reddy, Radha Gupta and C. G. Jagannatha

ABSTRACT: This research investigates the aligned magnetohydrodynamic (MHD) mixed convective flow behaviour of a hybrid nanoliquid due to an inclined permeable plate. A hybrid nanoliquid, consisting of water as the base fluid with dispersed copper and aluminum oxide nanoparticles, is subjected to an aligned magnetic field that alters its flow behaviour. The flow is further influenced by constant wall temperature boundary conditions. The partial differential equations (PDEs) are reduced to a set of ordinary differential equations (ODEs) through similarity variables. The resulting equations are then solved using the reduced differential transform method (RDTM), and the solutions are validated through comparison with numerical results to ensure their accuracy and consistency. Graphical representations depict the influence of many parameters on the velocity and temperature profiles, as well as on the skin friction coefficient and Nusselt number. The results demonstrate that an increase in the alignment angle of the magnetic field elevates the velocity and decreases the temperature within the flow, concurrently augmenting the magnetic interaction and mixed convection characteristics.

Keywords: Hybrid nanofluid, inclined plate, mixed convection, MHD, reduced differential transform method.

Contents

Nomenclature

Symbol	Description	Symbol	Description
(u, v)	Velocity components	B	Magnetic field strength
K_p	Porosity parameter	c_p	Specific heat
M	Magnetic field parameter	ϱ	Density
Pr	Prandtl number	g	Acceleration due to gravity
μ	Dynamic viscosity	ν	Kinematic viscosity
β	Thermal expansion coefficient	k	Thermal conductivity
U_∞	Free stream velocity	$\mathcal{T}$	Temperature
ϕ	Solid volume fraction	σ	Electrical conductivity
γ	Inclination angle of the plate	λ	Mixed convection parameter
η	Similarity variable	Nu_x	Nusselt number
C_f	Skin-friction	(x, y)	Directions
Subscripts			
f	Fluid	nf	Nanofluid
hnf	Hybrid nanofluid	w	Wall
∞	Ambient		

2020 *Mathematics Subject Classification:* 76W05, 76M10, 76S05.
Submitted January 31, 2026. Published April 30, 2026.

1. Introduction

The most challenging uses of nanofluids in engineering and research are of significant significance. The use of nanotechnology in modern science has prompted researchers to explore nanofluid (NF) models from various perspectives. NFs consist of nanoparticles ranging from 1 to 100 nm dispersed in a base fluid. The size of nanoparticles is selected to be diminutive because smaller particles possess a higher surface area relative to larger particles of the same mass. The release of ions from the surface area is directly proportional to the surface area; a larger surface area results in a higher release of ions. The primary reason nanoparticles are considered diminutive in size is their enhanced antibacterial efficacy, since they discharge a greater quantity of ions per unit mass compared to bigger particles. A hybrid NF consists of two distinct nanosized particles integrated with a base liquid. Aside from its very high thermal conductivity, hybrid NF offers significant advantages when the nanosized particles are properly disseminated. A hybrid NF has been created to examine and enhance heat transfer capabilities. Hybrid NFs have applications in heat transfer within microelectronics, microfluidics, manufacturing, and medicine. Reddy [1] examined the consequence of entropy generation on the radiative stagnation point motion of a hybrid NF. Mahood et al. [2] elucidate the radiative hybrid NF flow due to a wedge. Radhika and Reddy [3] deliberated the radiaive hybrid NF stream past an expandable surface. Farooq et al. [4] probed the heat transmission and hybrid NF stream over a spinning disk. Anjum et al. [5] scrutinized the radiative hybrid NF motion across a stretching surface.

Extensive theoretical and empirical research has been conducted on boundary layer flow approximation over a flat plate in both horizontal and vertical orientations. Nonetheless, there appears to be minimal investigation into inclined flat plates for hybrid NFs. This approximation is commonly found in engineering systems such as solar water heaters and inclination sensors, making it critical to investigate the flow on an inclined plate at various angles. Guo et al. [6] examined the liquid stream due to an inclined plate with a magnetic field. Kodi and Mopuri [7] studied the consequences of a chemical reaction on Casson fluid motion past an inclined plate. Ramzan et al. [8] examined the reactive Casson liquid sream past an inclined plate. Raza et al. [9] analyzed the convective nanoliquid motion past a permeable inclined plate. Riaz et al. [10] investigated the mass transfer and heat transfer in an Oldroyd-B liquid motion due to an inclined plate. Mixed convection heat transfer research has received a lot of attention in recent years due to its wide range of applications, such as density-driven circulation in lakes caused by seasonal changes, temperature variations in atmospheric flows, and heat exchangers in nuclear reactor fuel systems. The major feature of mixed convection is the buoyant force caused by density and temperature variations. Mathematically, according to Boussinesq's theory, the momentum and energy equations governing mixed convection are significantly interrelated. Prandtl's boundary layer theory posits that a fluid exhibiting mixed convection will generate a boundary layer next to the plate as a result of the fluid's viscosity. Ahmed et al. [11] investigated the mixed convective Williamson liquid stream with a curved surface. Hussain et al. [12] investigated the mixed convective Williamson fluid motion via a permeable wedge with a magnetic field. Taher et al. [13] studied heat transmission and Poiseuille-Rayleigh-Bénard mixed convection in a channel. Pandey et al. [14] investigated how radiation affects a mixed convective Newtonian liquid stream with a stretchable surface. Abbas et al. [15] investigated the effects of chemical reactions on mixed convective flow between concentric cylinders.

Magnetohydrodynamics (MHD) examines electrically conductive fluids inside a magnetic field. Recent research on electrically conducting streams shows that the introduction of a magnetic field greatly modifies their heat transfer characteristics. Fluid flow in a magnetic field has several practical applications, including power generators, nuclear reactors, and heat exchangers. Several research investigated the effects of a magnetic field on a nanofluid. Sarada et al. [16] investigated the effect of MHD on the non-Newtonian flow past an expandable surface. Yusuf et al. [17] studied the heat transmission and MHD flow of a Sisko liquid stream across inclined permeable walls. Rehman et al. [18] deliberated the MHD Carreau liquid stream past a stretchable sheet in the presence of radiation. Sarma and Sarma [19] elucidated the bioconvective MHD Casson liquid motion due to a stretchy surface. Azar et al [20] scrutinized the MHD Casson liquid motion past a permeable stretching/shrinking channel. The differential transformation method (DTM) is an innovative technique for addressing highly non-linear ODEs. While the Taylor series technique provided the basis for its development, it differs from conventional Taylor series methods, offering both a polynomial order solution and an accurate approximation of the needed differentiable

solution. Conversely, the DTM provides an iterative approach for deriving higher-order Taylor series, since the computation of higher-order derivatives becomes more complex within the Taylor series framework. In conjunction with differential equations, the DTM produces an analytical solution expressed as a power series. Keimanesh et al. [21] examined the non-Newtonian liquid motion between parallel plates with the aid of the DTM. Abazari and Soltanalizadeh [22] investigated the applications of DTM on the Kawahara equations. Hatami et al. [23] deliberated the Newtonian and non-Newtonian liquid motion between two horizontal plates using DTM. Mirzaaghaian and Ganji et al. [24] studied the application of DTM in the study of micropolar liquid motion across permeable walls. Pooja et al. [25] utilized DTM to investigate the Darcy-Forchheimer nanoliquid motion with convective boundary conditions.

The present study examines the aligned MHD mixed convection flow of hybrid NF over an inclined porous plate under isothermal wall conditions. The influences of aligned angle interaction, magnetic interaction, mixed convection parameter, inclination angle, nanoparticle volume fraction, and porous medium permeability on velocity, temperature distribution, skin-friction coefficient, and local Nusselt number are examined. The PDEs are reduced to ODEs using similarity transformations and solved using the RDTM. This analytical technique is based on the Taylor series expansion and offers an efficient and accurate method to address linear as well as nonlinear differential equations. RDTM has been successfully implemented for multiple differential equations, including boundary value problems and fractional systems. Thus, the results obtained from RDTM are validated against numerical results, demonstrating excellent agreement.

2. Mathematical Formulation

The study focuses on the two-dimensional, steady laminar mixed convective hybrid NF stream past an inclined porous plate, under the influence of an aligned magnetic field with the flow direction. The plate is held at a constant temperature $\mathcal{T}_w$ which exceeds the surrounding nanofluid's ambient temperature $\mathcal{T}_\infty$. The hybrid NF under consideration has water as the base fluid with copper (Cu) and aluminum oxide (Al_2O_3) nanoparticles dispersed within it. These nanoparticles are considered to be spherical in shape, and they are thermally in equilibrium with the base fluid. The magnetic field is aligned at an angle α to the vertical flow direction. The magnetic field strength varies with distance from the origin and is given by $B = \frac{B_0}{\sqrt{x/l}}$, $B_0 \neq 0$. Where B_0 is a constant representing the magnetic field strength, l is the characteristic length of the plate, and x denotes the spatial coordinate taken along the direction of the plate. The system is modeled with boundary conditions that assume constant temperature at the plate's surface and variable temperature in the surrounding fluid. The physical setup of the hybrid NF flow influenced by MHD over an inclined porous plate is shown in Figure 1. Interactions with the magnetic field, the porous medium, and the thermal boundary conditions influence the flow dynamics.

The following governing equations describe boundary layer flow (See [26,27,28]):

$$\frac{\partial u}{\partial x} + \frac{\partial v}{\partial y} = 0, \tag{2.1}$$

$$\varrho_{hnf}\left(u\frac{\partial u}{\partial x} + v\frac{\partial u}{\partial y}\right) = \mu_{hnf}\frac{\partial^2 u}{\partial y^2} + (\varrho\beta)_{hnf} g\cos\gamma(\mathcal{T} - \mathcal{T}_\infty) - \left(\sigma_{hnf}B^2(x) + \frac{\mu_{hnf}}{k^*}\right)\sin^2\alpha(u - U_\infty), \tag{2.2}$$

$$u\frac{\partial \mathcal{T}}{\partial x} + v\frac{\partial \mathcal{T}}{\partial y} = \alpha_{hnf}\frac{\partial^2 \mathcal{T}}{\partial y^2}. \tag{2.3}$$

The boundary conditions applied in this study are

$$\begin{aligned} y = 0: &\quad u = 0, \quad v = 0, \quad \mathcal{T} = \mathcal{T}_w. \\ y \to \infty: &\quad u \to U_\infty, \quad \mathcal{T} \to \mathcal{T}_\infty. \end{aligned} \tag{2.4}$$

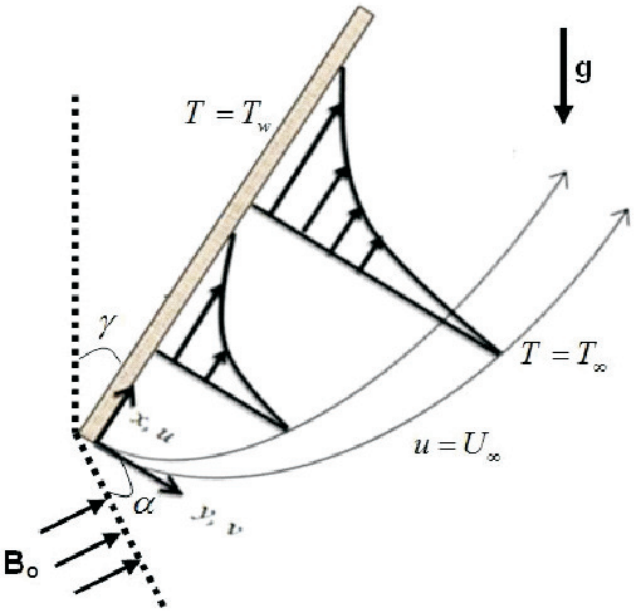

Figure 1: Flow geometry.

Table 1: Thermophysical characteristics of the hybrid nanofluid (see [28]).

Properties	Base Fluid (Water)	Al_2O_3 (Aluminium Oxide)	Cu (Copper)
ϱ (kg/m^3)	997.1	3970	8933
c_p (J/kg.K)	4179	765	385
k (W/m.K)	0.6071	40	400
$\beta \times 10^{-5}$ (1/K)	0.000256	0.000051	0.0000765
Pr	6.2		

The relevant thermophysical parameters of the hybrid nanofluid are given by,

$$\left.\begin{aligned}
\frac{k_{hnf}}{k_f} &= \frac{k_{\mathrm{Cu}}+2k_{nf}-2\phi_{\mathrm{Cu}}(k_{bf}-k_{\mathrm{Cu}})}{k_{\mathrm{Cu}}+2k_{nf}+\phi_{\mathrm{Cu}}(k_{bf}-k_{\mathrm{Cu}})} \times \frac{k_{\mathrm{Al_2O_3}}+2k_f-2\phi_{\mathrm{Al_2O_3}}(k_f-k_{\mathrm{Al_2O_3}})}{k_{\mathrm{Al_2O_3}}+2k_f+\phi_{\mathrm{Al_2O_3}}(k_f-k_{\mathrm{Al_2O_3}})},\\
\frac{(\rho c_p)_{hnf}}{(\rho c_p)_f} &= (1-\phi_{\mathrm{Cu}})\left[(1-\phi_{\mathrm{Al_2O_3}})+\phi_{\mathrm{Al_2O_3}}\left(\frac{(\rho c_p)_{\mathrm{Al_2O_3}}}{(\rho c_p)_f}\right)\right]+\phi_{\mathrm{Cu}}\frac{(\rho c_p)_{\mathrm{Cu}}}{(\rho c_p)_f},\\
\frac{(\rho\beta)_{hnf}}{(\rho\beta)_f} &= (1-\phi_{\mathrm{Cu}})\left[(1-\phi_{\mathrm{Al_2O_3}})+\phi_{\mathrm{Al_2O_3}}\left(\frac{(\rho\beta)_{\mathrm{Al_2O_3}}}{(\rho\beta)_f}\right)\right]+\phi_{\mathrm{Cu}}\frac{(\rho\beta)_{\mathrm{Cu}}}{(\rho\beta)_f},\\
\frac{\sigma_{hnf}}{\sigma_f} &= \frac{\sigma_{\mathrm{Cu}}+2\sigma_{nf}-2\phi_{\mathrm{Cu}}(\sigma_{nf}-\sigma_{\mathrm{Cu}})}{\sigma_{\mathrm{Cu}}+2\sigma_{nf}+\phi_{\mathrm{Cu}}(\sigma_{nf}-\sigma_{\mathrm{Cu}})} \times \frac{\sigma_{\mathrm{Al_2O_3}}+2\sigma_f-2\phi_{\mathrm{Al_2O_3}}(\sigma_f-\sigma_{\mathrm{Al_2O_3}})}{\sigma_{\mathrm{Al_2O_3}}+2\sigma_f+\phi_{\mathrm{Al_2O_3}}(\sigma_f-\sigma_{\mathrm{Al_2O_3}})},\\
\frac{\rho_{hnf}}{\rho_f} &= \left\{(1-\phi_{\mathrm{Cu}})\left[(1-\phi_{\mathrm{Al_2O_3}})+\phi_{\mathrm{Al_2O_3}}\left(\frac{\rho_{\mathrm{Al_2O_3}}}{\rho_f}\right)\right]+\phi_{\mathrm{Cu}}\frac{\rho_{\mathrm{Cu}}}{\rho_f}\right\},\\
\frac{\mu_{hnf}}{\mu_f} &= \frac{1}{(1-\phi_{\mathrm{Al_2O_3}})(1-\phi_{\mathrm{Cu}})}.
\end{aligned}\right\} \tag{2.5}$$

$$A_1 = \frac{\mu_{hnf}}{\mu_f},\quad A_2 = \frac{\rho_{hnf}}{\rho_f},\quad A_3 = \frac{(\rho c_p)_{hnf}}{(\rho c_p)_f},\quad A_4 = \frac{k_{hnf}}{k_f},\quad A_5 = \frac{\sigma_{hnf}}{\sigma_f},\quad A_6 = \frac{(\rho\beta)_{hnf}}{(\rho\beta)_f}.$$

The relevant thermophysical characteristics of the base fluid, copper, and alumina nanoparticles used in this study are listed in Table 1.

2.1. Similarity Conversion

In terms of the stream function $\psi(x,y)$, the velocity components u and v are given by:

$$u = \frac{\partial \psi}{\partial y}, \qquad v = -\frac{\partial \psi}{\partial x}. \tag{2.6}$$

The dimensionless transformation is introduced as follows

$$\begin{aligned} \eta &= y\left(\frac{U_\infty}{\nu_f x}\right)^{1/2} = \frac{y}{x}\sqrt{Re_x} = \frac{y}{x}\left(\frac{U_\infty x}{\nu_f}\right)^{1/2}, \\ \psi(x,y) &= \nu_f \sqrt{Re_x}\ f(\eta) = \sqrt{U_\infty \nu_f x}\ f(\eta), \\ \theta(\eta) &= \frac{\mathcal{T}-\mathcal{T}_\infty}{\mathcal{T}_w-\mathcal{T}_\infty}. \end{aligned} \tag{2.7}$$

The Reynolds number is expressed as $Re_x = U_\infty x/\nu_f$. By applying the dimensionless transformation (2.7) satisfy (2.1) and (2.2)–(2.4) are transformed into the following system of non-dimensional ordinary differential equations.

$$\frac{A_1}{A_2} f'''(\eta) + \frac{1}{2} f''(\eta) f(\eta) + \frac{A_6}{A_2}\lambda \cos\gamma\ \theta(\eta) - \left(\frac{A_5}{A_2}M + \frac{A_1}{A_2}K_p\right)\sin^2\alpha(f'(\eta)-1) = 0. \tag{2.8}$$

$$\frac{A_4}{A_3}\theta''(\eta) + \Pr\frac{1}{2} f(\eta)\theta'(\eta) = 0. \tag{2.9}$$

For this formulation, primes represent derivatives with respect to η. The derived system of equations can be further simplified and solved numerically to obtain the velocity and temperature profiles.

Where

$$\lambda = \frac{g\beta_f(\mathcal{T}_w-\mathcal{T}_\infty)x}{U_\infty^2}, \qquad M = \frac{\sigma B_0^2 l}{\varrho_f U_\infty}, \qquad K_p = \frac{\nu_f x}{k^* U_\infty}, \qquad \Pr = \frac{(\mu c_p)_f}{k_f}, \qquad \nu_f = \frac{\mu_f}{\varrho_f}.$$

The non-dimensionalized boundary conditions are expressed as

$$\begin{array}{llll} f(0) = 0, & f'(0) = 0, & \theta(0) = 1 & \text{at} \quad \eta = 0 \\ f'(\eta) \to 1, & \theta(\eta) \to 0 & & \text{as} \quad \eta \to \infty. \end{array} \tag{2.10}$$

The local skin-friction coefficient, C_f and the local Nusselt number, Nu_x are defined as

$$C_f = \frac{\tau_w}{\varrho_f U_\infty^2}, \qquad Nu_x = \frac{q_w x}{k_f(\mathcal{T}_w-\mathcal{T}_\infty)}. \tag{2.11}$$

The symbol τ_w is the wall shear stress, while q_w stands for heat flux from the plate and are expressed as

$$\tau_w = \mu_{hnf}\left(\frac{\partial u}{\partial y}\right)_{y=0}, \qquad q_w = -k_{hnf}\left(\frac{\partial \mathcal{T}}{\partial y}\right)_{y=0}. \tag{2.12}$$

Substituting (2.7) and (2.12) into (2.11) yields the following non-dimensional forms.

$$C_f Re_x^{1/2} = \frac{1}{(1-\phi_1)^{2.5}(1-\phi_2)^{2.5}} f''(0), \qquad Nu_x Re_x^{-1/2} = -\frac{k_{hnf}}{k_f}\left(\theta'(0)\right). \tag{2.13}$$

3. Reduced Differential Transform Method (RDTM)

Based on the fundamental principles of the one-dimensional differential transform method (DTM), a function of two variables can be composed of two components, each related to a single variable. This

representation is given by

$$f(\xi,\tau) = \left(\sum_{m=0}^{\infty} G(m)\xi^m\right)\left(\sum_{n=0}^{\infty} G(n)\xi^n\right)$$
$$= \sum_{k=0}^{\infty} F_k(\xi)\tau^k, \tag{3.1}$$

where $F_k(\xi)$ denotes the spectrum of $f(\xi,\tau)$ with respect to τ.

Definition 3.1 (see [29]) *Let $f(\xi,\tau)$ be an analytic function of two variables, continuously differentiable in ξ and τ over the domain. The reduced differential transform of $f(\xi,\tau)$, denoted as $F_k(\xi)$, is defined by*

$$F_k(\xi) = \frac{1}{k!}\left[\frac{\partial^k f(\xi,\tau)}{\partial\tau^k}\right]_{\tau=0}. \tag{3.2}$$

Here $F_k(\xi)$ is the transformed function derived from the original function $f(\xi,\tau)$.

Definition 3.2 (see [29]) *The inverse differential transform is used to recover the original function from its transformed components and is expressed as*

$$f(\xi,\tau) = \sum_{k=0}^{\infty} F_k(\xi)\tau^k. \tag{3.3}$$

By combining (3.1) and (3.2), an equivalent representation is derived as

$$f(\xi,\tau) = \sum_{k=0}^{\infty}\left(\frac{1}{k!}\left[\frac{\partial^k f(\xi,\tau)}{\partial\tau^k}\right]_{\tau=0}\right)\tau^k. \tag{3.4}$$

To illustrate the fundamentals of RDTM, we analyze a nonlinear PDE formulated in operator notation:

$$L[f(\xi,\tau)] + R[f(\xi,\tau)] + N[f(\xi,\tau)] = g(\xi,\tau), \tag{3.5}$$

with initial condition

$$f(\xi,0) = h(\xi). \tag{3.6}$$

Here, L is a linear operator, typically involving partial derivatives; N is a nonlinear operator and $g(\xi,\tau)$ denotes a known inhomogeneous source term.

Following the standard RDTM procedure, we derive the recursive relation

$$(k+1)F_{k+1}(\xi,\tau) = G_k(\xi) - RF_k(\xi) - NF_k(\xi), \tag{3.7}$$

where $F_k(\xi)$, $RF_k(\xi)$, $NF_k(\xi)$ and $G_k(\xi)$ are the differential transforms of $f(\xi,\tau)$, $R[f(\xi,\tau)]$, $N[f(\xi,\tau)]$ and $g(\xi,\tau)$, respectively.

The initial condition (3.6) is transformed as

$$F_0(\xi) = h(\xi). \tag{3.8}$$

By substituting (3.7) iteratively, we can determine the transformed components $F_k(\xi)$. The approximate solution is then obtained using the inverse transform,

$$f_n(\xi,\tau) = \sum_{k=0}^{\infty} F_k(\xi)\tau^k. \tag{3.9}$$

As $n\to\infty$, this yields the exact solution of the given problem

$$f(\xi,\tau) = \lim_{n\to\infty} f_n(\xi,\tau). \tag{3.10}$$

Theorem 3.1 *Let $f(\xi,\tau)$, $g(\xi,\tau)$, and $h(\xi,\tau)$ be three analytic functions such that $F_k(\xi)$, $G_k(\xi)$ and $H_k(\xi)$ are their corresponding reduced differential transforms. Table 2 lists the basic operational rules of RDTM.*

Table 2: Basic operations involved in the RDTM (see [29]).

Function Form	Transformed Form
1. $g(\xi,\tau)=\phi(\xi,\tau)\pm\psi(\xi,\tau)$	$G_n(\xi)=\Phi_n(\xi)\pm\Psi_n(\xi)$
2. $g(\xi,\tau)=a\cdot\phi(\xi,\tau)$	$G_n(\xi)=a\cdot\Phi_n(\xi)$, where a is a constant
3. $g(\xi,\tau)=\dfrac{\partial\phi(\xi,\tau)}{\partial\xi}$	$G_n(\xi)=\dfrac{\partial\Phi_n(\xi)}{\partial\xi}$
4. $g(\xi,\tau)=\dfrac{\partial^n\phi(\xi,\tau)}{\partial\tau^n}$	$G_n(\xi)=(n+1)\dots(n+r)\Phi_{n+r}(\xi)$ or $G_n(\xi)=\dfrac{(n+r)!}{n!}\cdot\Phi_{n+r}(\xi)$
5. $g(\xi,\tau)=\xi^p\tau^q$	$G_n(\xi)=\xi^p\delta(n-q)$, where δ is the Kronecker delta
6. $g(\xi,\tau)=\xi^p\tau^q\phi(\xi,\tau)$	$G_n(\xi)=\xi^p\Phi_{n-q}(\xi)$
7. $g(\xi,\tau)=\phi(\xi,\tau)\cdot\psi(\xi,\tau)$	$G_n(\xi)=\sum_{s=0}^{n}\Phi_s(\xi)\Psi_{n-s}(\xi)$
8. $g(\xi,\tau)=\dfrac{\partial^{r+s}\phi(\xi,\tau)}{\partial\xi^r\partial\tau^s}$	$G_n(\xi)=\dfrac{(n+s)!}{n!}\cdot\dfrac{\partial^r}{\partial}\xi^r\Phi_{n+s}(\xi)$

4. Application of RDTM

Applying the RDTM to the nonlinear equations (2.8) and (2.9) yields the following results:

$$\frac{A_1}{A_2}\,(q+1)(q+2)(q+3)F[q+3]+\frac{1}{2}\sum_{r=0}^{q}F[q-r](r+1)(r+2)F[r+2]+\frac{A_6}{A_2}\,\lambda\cos\gamma\;\theta[q]$$
$$-\left(\frac{A_5}{A_2}\,M+\frac{A_1}{A_2}\,K_p\right)\sin^2\alpha((q+1)F[q+1]-1)=0. \tag{4.1}$$

$$\frac{A_4}{A_3}(q+1)(q+2)\theta[q+2]+\frac{\Pr}{2}\sum_{r=0}^{q}\,F[q-r](r+1)\theta[r+1]=0. \tag{4.2}$$

Rearranging the above, the recursive formulas become

$$F[q+3]=-\frac{A_2}{A_1(q+1)(q+2)(q+3)}\left(\frac{1}{2}\,\sum_{r=0}^{q}F[q-r](r+1)(r+2)F[r+2]\right.$$
$$\left.+\frac{A_6}{A_2}\lambda\cos\gamma\;\theta[q]-\left(\frac{A_5}{A_2}M+\frac{A_1}{A_2}K_p\right)\sin^2\alpha((q+1)F[q+1]-1)\right). \tag{4.3}$$

$$\theta[q+2]=-\frac{A_3}{A_4\;(q+1)(q+2)}\cdot\frac{\Pr}{2}\;\sum_{r=0}^{q}F[q-r](r+1)\theta[r+1]. \tag{4.4}$$

The boundary conditions from (2.10) transform into

$$F(0)=0,\quad F(1)=0,\quad F(2)=A;\qquad \theta(0)=1,\quad \theta(1)=B. \tag{4.5}$$

Using the iterative formulas (4.3) and (4.4), we obtain the successive approximation as

$$F(3) = -\frac{1}{6}(A_6\ \lambda\cos\gamma + (A_1A_5\ M + K_p)\ \sin^2\alpha), \tag{4.6}$$

$$F(4) = -\frac{1}{24}(A_6\ \lambda\cos\gamma \cdot B + (A_1A_5\ M + K_p)\sin^2\alpha(2A-1)), \tag{4.7}$$

$$F(5) = -\frac{1}{60}(A_1A_2A^2 + A_6\lambda\cos\gamma\theta(2) - (A_1A_5M + K_p)\sin^2\alpha \left(-\frac{1}{2}(A_6\ \lambda\cos\gamma + (A_1A_5M + K_p)\sin^2\alpha - 1)\right), \tag{4.8}$$

and so on.

$$\theta(2) = 0, \tag{4.9}$$

$$\theta(3) = 0, \tag{4.10}$$

$$\theta(4) = -\frac{1}{24} \cdot \frac{A_3}{A_4} \cdot \Pr \cdot BA, \tag{4.11}$$

$$\theta(5) = \frac{1}{240}\left(\frac{A_3A_6}{A_4} \cdot \Pr \cdot B(\lambda\cos\gamma + (A_1A_5M + K_p)\sin^2\alpha)\right), \tag{4.12}$$

and so on.

Here, $\theta[k]$ represents the differential transform of $\theta(\eta)$, while A and B are constants to be determined by applying the boundary conditions. Based on (4.5)–(4.12), a fifth-order power series has been developed as follows:

$$\begin{aligned} f(\eta) = {} & 0.0002319553247\ \eta^2((1.540646743 \times 10^{10})A\ \eta^4 + (1.69333 \times 10^8)A^2\ \eta^3 \\ & - (1.15890 \times 10^8)\ A^2\eta^3 + (2.64545 \times 10^7)A^2\ \eta^3 + 1.09638A\ \eta^2 + 4\ \eta + 0.20\ \eta^2 \\ & - 2.5\ A\ \eta^2 + 0.21065\ \eta^3 - 0.51926\ \eta + 0.02921\ \eta^3 - 1.03852\ \eta^2 - 2.19076\ \eta \\ & + (7.39287 \times 10^8)A - (8.24431 \times 10^8)\ A^2\eta^3 - (2.10963 \times 10^9)\ A + 0.25278\ \eta^2) \end{aligned} \tag{4.13}$$

$$\begin{aligned} \theta(\eta) = {} & 1 + B\ \eta - 0.1502807146\ B\ A\ \eta^4 - 0.002515571\ B\ \eta^5 - 0.002368519\ B\ \eta^5 \\ & + 0.02717086727\ B\ \eta^5 + 0.013913503\ BA\ \eta^4 + 0.000219286\ B\ \eta^5 \end{aligned} \tag{4.14}$$

The constants A and B are determined by applying the RDTM to (4.13) and (4.14), along with the boundary conditions in (2.10). Substituting the obtained values $A = 0.5364712662$ and $B = -1.053354241$ into the series expressions (4.13) and (4.14) yields:

$$\begin{aligned} f(\eta) = {} & (7.233750575 \times 10^{-11})\ \eta^2((7.416225650 \times 10^9) \\ & - (2.016727850 \times 10^8)\ \eta^3 - 1.223165230\ \eta^2 + 3.5870\ \eta). \end{aligned} \tag{4.15}$$

$$\theta(\eta) = 1.000000000 - 1.053354241\ \eta + 0.7690526777\ \eta^4 - 0.2355102735\ \eta^5. \tag{4.16}$$

5. Results and Discussions

This section studies how the impact of various parameters affects the dimensionless velocity $f'(\eta)$, temperature distribution $\theta(\eta)$, skin friction coefficient, and the Nusselt number in hybrid nanofluid flow past an inclined porous plate in a porous medium. The hybrid nanofluid we are examining, with water as its base and mixed with copper (Cu) and aluminum oxide (Al_2O_3) nanoparticles, is placed in the presence of an aligned magnetic field. The nonlinear equations governing the flow are solved using the Reduced Differential Transform Method (RDTM) and the results are verified through comparison with numerical

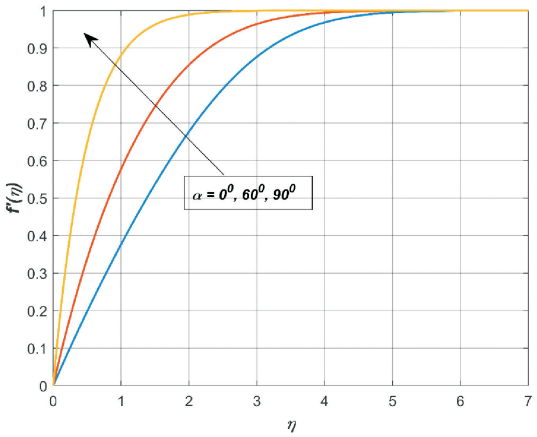

Figure 2: Impact of α on $f'(\eta)$.

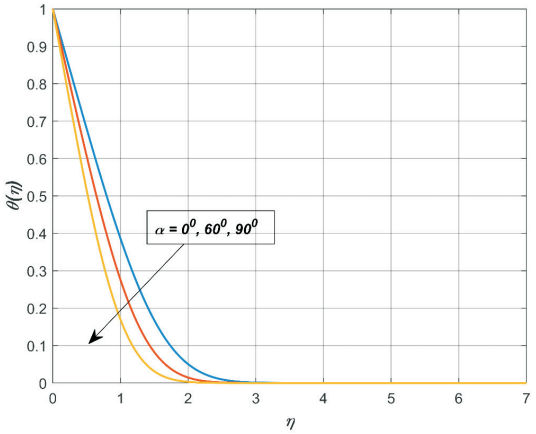

Figure 3: Impact of α on $\theta(\eta)$.

simulations. For numerical computations, the nondimensional parameters are fixed as $\alpha = 90°$, $M = 1$, $\gamma = 45°$, $\phi_1 = \phi_2 = 0.1$, $\lambda = 1$, $K_p = 1$ and $\Pr = 6.2$. In this study, $\gamma = 0°$ corresponds to a static vertical plate, while $\gamma = 90°$ corresponds to a static horizontal plate.

Comparative data in Table 3 reveal that the DTM results exhibit closer agreement with the numerical solution compared to the Runge-Kutta 4th order (RK-4) method, confirming the reliability of RDTM for subsequent analysis. In Table 4, validation of the skin friction coefficient and Nusselt number values for various values of ϕ_1 is provided by comparison with existing literature, while Table 5 illustrates the effect of dimensionless parameters on these quantities. Figures 2a and 2b demonstrate the effect of the magnetic field inclination angle α on the dimensionless velocity and temperature distributions. An increase in α enhances the velocity profile while simultaneously reducing the temperature. Figure 2 shows how increasing the magnetic field inclination angle (α) considerably influences the velocity profile. As α increases from 0° to 90°, the velocity profile intensifies and reaches the free-stream value at lower values of η. This behaviour indicates a decrease in the thickness of the momentum boundary layer. In physical terms, the inclination of the magnetic field decreases the effective Lorentz force acting against the flow direction, lowering magnetic resistance. As a result, fluid motion increases, resulting in higher velocities and faster momentum diffusion inside the boundary layer region. Figure 3 shows the effect of α on temperature distribution. It is found that raising the inclination angle results in a significant reduction in the thermal profile and thinning of the thermal boundary layer. Higher α values reduce magnetic damping, increasing fluid velocity while encouraging convective heat transport away from the surface. As a result, heat circulates more efficiently into the fluid, lowering temperature levels inside the boundary layer. This finding emphasises the critical importance of magnetic field direction in regulating thermal behaviour and heat transfer performance. Table 5 indicates that higher values of α produce higher skin friction coefficients and Nusselt numbers for the hybrid nanofluid.

Figure 4 demonstrates how the velocity profile fluctuates with various values of the magnetic parameter M. It is evident that increasing M improves velocity, causing the profile to approach the free-stream value more quickly. This reveals a decline in the thickness of the momentum boundary layer. Physically, the magnetic field produces a Lorentz force, but the present design enables the induced motion to assist with the flow, enhancing liquid acceleration close to the surface. As a consequence, stronger magnetic intensity accelerates momentum transfer and boosts overall fluid velocity. Figure 5 depicts the impact of M on the temperature distribution $\theta(\eta)$. As the magnetic parameter expands, the thermal profile diminishes, and the thermal boundary layer weakens. This behaviour indicates that heat is being eliminated from the surface more successfully. The strengthened magnetic field raises fluid velocity, accelerating convective heat transfer and permitting thermal energy to circulate more quickly into the fluid around it. As it turns out, with a greater value of M, the temperature within the boundary layer reduces rapidly, illustrating the magnetic field's significance in governing thermal transport. Table 5 also

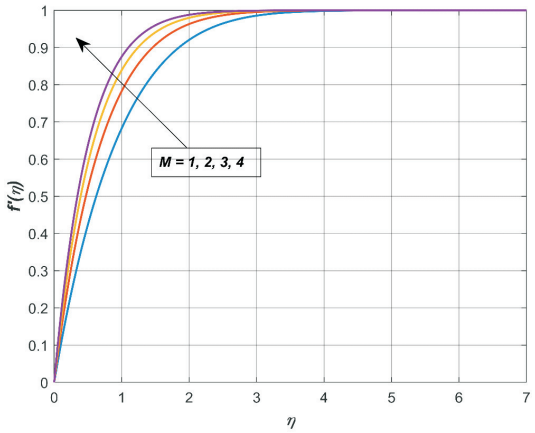

Figure 4: Impact of M on $f'(\eta)$.

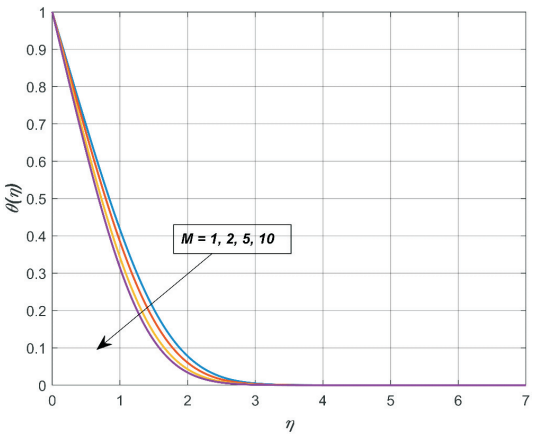

Figure 5: Impact of M on $\theta(\eta)$.

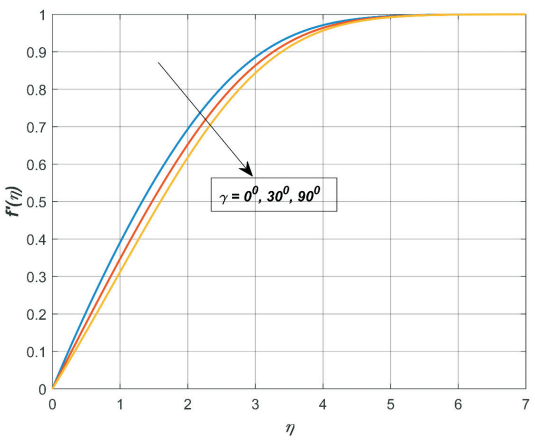

Figure 6: Impact of γ on $f'(\eta)$.

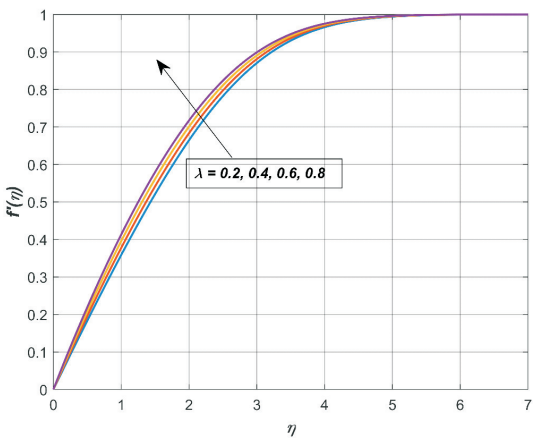

Figure 7: Impact of λ on $f'(\eta)$.

proves that an increase in M causes both the skin friction coefficient and the Nusselt number to rise for the hybrid nanofluid. Figure 6 demonstrate how the inclination angle γ affects the velocity profile. As γ increases, the velocity of the flow drops. At $\gamma = 90°$, the gravitational force acts normal to the plate surface, eliminating the buoyancy effect since $\cos(90°) = 0$. In contrast, at $\gamma = 0°$, the gravitational force is aligned along the plate surface, maximizing the buoyancy effect with $\cos(90°) = 1$. This enhanced vertical driving force thickens the velocity and thins the thermal boundary layer as γ increases.

Figure 7 depicts the consequence of the λ on the velocity profile. Boosting λ raises velocity over the boundary layer. Increased λ values improve fluid momentum, which leads to velocity attaining the free-stream state at reduced η values. This behaviour reveals a reduction of the momentum boundary layer. In principle, stronger unsteady effects minimise flow resistance while boosting momentum diffusion, elevating the flow's overall intensity close to the surface. Figure 8 displays how the temperature profile fluctuates according to different λ values. As λ rises, the temperature of the boundary layer drops steadily yet consistently, which is apparent in the figure. The aforementioned pattern reflects a drop in thermal boundary layer thickness. Higher unsteadiness increases fluid motion, which accelerates convective transfer of heat and facilitates faster elimination of heat from the surface. A greater number of λ leads to stronger thermal diffusion and less heat across the flow region. We see from Table 5 that a rise in λ is linked to better C_f and Nu_x values.

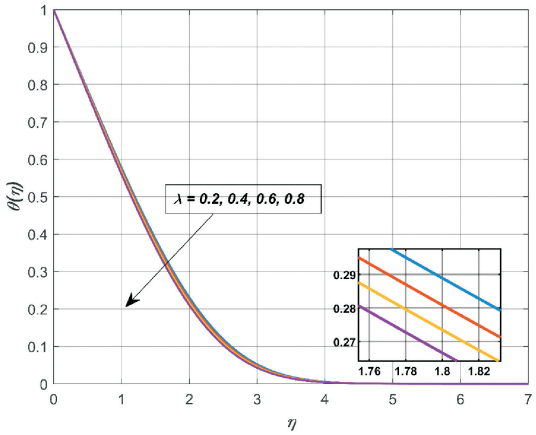

Figure 8: Impact of λ on $\theta(\eta)$.

Table 3: Comparison of numerical results and RDTM solutions along with the absolute errors.

	$f'(\eta)$			$\theta(\eta)$		
η	NM	RDTM	Error	NM	RDTM	Error
0.0	0.00000	0.00000	0.00000	1.00000	1.00000	0.00000
0.1	0.10374	0.18506	0.08132	0.88404	0.87193	0.01211
0.2	0.20743	0.34334	0.13591	0.76840	0.74425	0.02415
0.3	0.31093	0.47777	0.16684	0.65387	0.61798	0.03589
0.4	0.41399	0.59133	0.17734	0.54164	0.49480	0.04684
0.5	0.51630	0.68698	0.17068	0.43317	0.37706	0.05611
0.6	0.61745	0.76766	0.15021	0.33008	0.26782	0.06226
0.7	0.71696	0.83635	0.11939	0.23395	0.17077	0.06318
0.8	0.81428	0.89600	0.08172	0.14622	0.09030	0.05592
0.9	0.90883	0.94956	0.04073	0.06801	0.03147	0.03654
1.0	1.00000	1.00000	0.00000	0.00000	0.00000	0.00000

Table 4: Comparison of skin friction coefficient and Nusselt number for various values of ϕ_1, considering $\phi_2 = 0$, $M = 0$, $\alpha = 0$, $\gamma = 0$, $\lambda = 0$, $K_p = 0$ and $k_{nf}/k_f = 1$ for Cu/Al_2O_3-Water hybrid nanofluids.

ϕ_1	Skin Friction $\lvert f''(0)\rvert$ [30]	Present $\lvert f''(0)\rvert$	Present $\theta'(0)$
0	0.3321	0.33206	0.62007
0.002	0.3355	0.33289	0.62058
0.004	0.3390	0.33372	0.62108
0.008	0.3459	0.33538	0.62209
0.010	0.3494	0.33621	0.62259
0.012	0.3528	0.33705	0.62309
0.014	0.3563	0.33788	0.62360
0.016	0.3597	0.33871	0.62410
0.018	0.3632	0.33955	0.62460
0.02	0.3667	0.34038	0.62510
0.1	0.5076	0.47407	0.64459
0.2	0.7066	0.69705	0.66769

Table 5: Effects of skin friction and Nusselt number for Cu/Al_2O_3 hybrid nanofluid with various parameter values.

α	M	γ	ϕ_1	ϕ_2	λ	K_p	$\lvert f''(0)\rvert$	$\theta'(0)$
0°	1	45°	0.1	0.1	1	0.5	0.43944	0.65367
45°							1.28323	0.82603
60°							1.54495	0.86064
90°							1.76878	0.88616
90°	0	45°	0.1	0.1	1	0.5	1.46846	0.85111
	1						1.76878	0.88616
	2						2.02537	0.91178
	3						2.25305	0.93185
90°	1	0°	0.1	0.1	1	0.5	1.92781	0.90587
		45°					1.84500	0.89586
		60°					1.76878	0.88616
		90°					1.69956	0.87693
90°	1	45°	0.0	0.0	1	0.5	1.92720	0.89527
			0.2	0.0			1.83808	0.88616
			0.1	0.1			1.69956	0.87396
90°	1	45°	0.1	0.1	0.1	0.5	1.37786	0.76543
					0.5		1.59688	0.79903
					1		1.95762	0.88660
					3		2.11679	0.90876
90°	1	45°	0.1	0.1	1	0.5	1.76878	0.88616
						0.625	1.65215	0.87328
						1	1.46002	0.85003
						2	1.27842	0.82533

6. Conclusion

This study investigates the flow characteristics of a hybrid nanofluid over an inclined permeable plate subjected to MHD mixed convection and porous medium. An aligned magnetic field alters the flow characteristics of a hybrid nanofluid composed of water as the base fluid, with suspended copper and aluminium oxide nanoparticles. A similarity transformation is employed to transform the governing nonlinear partial differential equations into nonlinear ordinary differential equations. The RDTM is utilised to resolve the resultant equations, and the accuracy and consistency of the outputs are validated through comparison with numerical data. The graphical illustration demonstrates the impact of various dimensionless parameters on fluid profiles. The primary outputs of the present issue are enumerated below.

- Increasing α raises the velocity and reduces the temperature, resulting in thinner momentum and thermal boundary layers.
- As M increases, velocity increases, and temperature decreases, leading to thinner boundary layers.
- Higher γ decreases velocity and increases temperature, with the buoyancy effect being maximum at $\gamma = 0°$.
- Increasing λ increases velocity and decreases temperature, resulting in thinner boundary layers.
- The skin friction coefficient and Nusselt number increase with increasing values of α, M, γ and λ, but decrease with increasing ϕ_1, ϕ_2 and K_p.

Data Availability Statement

Data will be made available on the request. We have used all the data graphically and numerically in our paper for publication, while the backup of the files would be available on request.

Acknowledgments

The authors thank the anonymous reviewers for their careful reading of our manuscript and their many insightful comments and suggestions.

References

1. P. B. A. Reddy, Biomedical aspects of entropy generation on electromagnetohydrodynamic blood flow of hybrid nanofluid with nonlinear thermal radiation and non-uniform heat source/sink, *Eur. Phys. J. Plus*, vol. 135, no. 10, p. 852, Oct. 2020, doi: 10.1140/epjp/s13360-020-00825-7.

2. F. Mabood, A. Shafiq, W. A. Khan and I. A. Badruddin, MHD and nonlinear thermal radiation effects on hybrid nanofluid past a wedge with heat source and entropy generation, *Int. J. Numer. Methods Heat Fluid Flow*, vol. 32, no. 1, pp. 120–137, May 2021, doi: 10.1108/HFF-10-2020-0636.

3. M. Radhika and Y. Dharmendar Reddy, Thermal radiation and heat source/sink influence on MHD heat transmission of copper (Cu)–aluminum oxide (Al2O3) Hybrid nanofluid flow with velocity and thermal slips along a stretching sheet, *Radiat. Eff. Defects Solids*, vol. 179, no. 11–12, pp. 1656–1682, Nov. 2024, doi: 10.1080/10420150.2024.2359695.

4. U. Farooq, M. Imran, S. Noreen, N. Fatima and T. Muhammad, Heat Transfer Performance of Hybrid Nanofluid Radiative Flow via a Rotating Disk With Heat Source–Sink Effects and Response Surface Methodology, *Math. Methods Appl. Sci.*, vol. n/a, no. n/a, doi: 10.1002/mma.10821.

5. A. Anjum, Ch. Maheswari, B. N. Lakshmi, R. M. Ramana, S. Peerusab and S. A. Gaffar, Computational study of magnetized 3D revolving hybrid nanofluid with non-linear thermal radiation and heat source/sink over a stretching sheet, *Multiscale Multidiscip. Model. Exp. Des.*, vol. 8, no. 3, p. 200, Feb. 2025, doi: 10.1007/s41939-025-00748-9.

6. B. Guo *et al.*, Fractional-order simulations for heat and mass transfer analysis confined by elliptic inclined plate with slip effects: A comparative fractional analysis, *Case Stud. Therm. Eng.*, vol. 28, p. 101359, Dec. 2021, doi: 10.1016/j.csite.2021.101359.

7. R. Kodi and O. Mopuri, Unsteady MHD oscillatory Casson fluid flow past an inclined vertical porous plate in the presence of chemical reaction with heat absorption and Soret effects, *Heat Transf.*, vol. 51, no. 1, pp. 733–752, 2022, doi: 10.1002/htj.22327.

8. M. Ramzan, A. Saeed, P. Kumam, Z. Ahmad, M. S. Junaid and D. Khan, Influences of Soret and Dufour numbers on mixed convective and chemically reactive Casson fluids flow towards an inclined flat plate, *Heat Transf.*, vol. 51, no. 5, pp. 4393–4433, 2022, doi: 10.1002/htj.22505.

9. A. Raza *et al.*, Significance of Free Convection Flow over an Oscillating Inclined Plate Induced by Nanofluid with Porous Medium: The Case of the Prabhakar Fractional Approach, *Micromachines*, vol. 13, no. 11, Art. no. 11, Nov. 2022, doi: 10.3390/mi13112019.

10. M. B. Riaz, A. Ur Rehman, A. Wojciechowski and A. Atangana, Heat and mass flux analysis of magneto-free-convection flow of Oldroyd-B fluid through porous layered inclined plate, *Sci. Rep.*, vol. 13, no. 1, p. 653, Jan. 2023, doi: 10.1038/s41598-022-27265-w.

11. K. Ahmed, W. A. Khan, T. Akbar, G. Rasool, S. O. Alharbi and I. Khan, Numerical Investigation of Mixed Convective Williamson Fluid Flow Over an Exponentially Stretching Permeable Curved Surface, *Fluids*, vol. 6, no. 7, Art. no. 7, Jul. 2021, doi: 10.3390/fluids6070260.

12. M. Hussain, S. Jahan, Q. A. Ranjha, J. Ahmad, M. K. Jamil and A. Ali, Suction/blowing impact on magneto-hydrodynamic mixed convection flow of Williamson fluid through stretching porous wedge with viscous dissipation and internal heat generation/absorption, *Results Eng.*, vol. 16, p. 100709, Dec. 2022, doi: 10.1016/j.rineng.2022.100709.

13. R. Taher, M. M. Ahmed, Z. Haddad and C. Abid, Poiseuille-Rayleigh-Bénard mixed convection flow in a channel: Heat transfer and fluid flow patterns, *Int. J. Heat Mass Transf.*, vol. 180, p. 121745, Dec. 2021, doi: 10.1016/j.ijheatmasstransfer.2021.121745.

14. A. K. Pandey *et al.*, Insight into the relationship between non-linear mixed convection and thermal radiation: The case of Newtonian fluid flow due to non-linear stretching, *Propuls. Power Res.*, vol. 12, no. 1, pp. 153–165, Mar. 2023, doi: 10.1016/j.jppr.2022.11.002.

15. Z. Abbas, I. Mehdi, J. Hasnain, A. K. Alzahrani and M. Asma, Homogeneous-heterogeneous reactions in MHD mixed convection fluid flow between concentric cylinders with heat generation and heat absorption, *Case Stud. Therm. Eng.*, vol. 42, p. 102718, Feb. 2023, doi: 10.1016/j.csite.2023.102718.

16. K. Sarada, R. J. P. Gowda, I. E. Sarris, R. N. Kumar and B. C. Prasannakumara, Effect of Magnetohydrodynamics on Heat Transfer Behaviour of a Non-Newtonian Fluid Flow over a Stretching Sheet under Local Thermal Non-Equilibrium Condition, *Fluids*, vol. 6, no. 8, Art. no. 8, Aug. 2021, doi: 10.3390/fluids6080264.

17. T. A. Yusuf, R. Naveen Kumar, R. J. Punith Gowda and U. D. Akpan, Entropy generation on flow and heat transfer of a reactive MHD Sisko fluid through inclined walls with porous medium, *Int. J. Ambient Energy*, vol. 43, no. 1, pp. 6307–6316, Dec. 2022, doi: 10.1080/01430750.2021.2013941.

18. M. I. Ur Rehman, H. Chen and A. Hamid, Multi-physics modeling of magnetohydrodynamic Carreau fluid flow with thermal radiation and Darcy–Forchheimer effects: a study on Soret and Dufour phenomena, *J. Therm. Anal. Calorim.*, vol. 148, no. 24, pp. 13883–13894, Dec. 2023, doi: 10.1007/s10973-023-12699-9.

19. A. K. Sarma and D. Sarma, Unsteady magnetohydrodynamic bioconvection Casson fluid flow in presence of gyrotactic microorganisms over a vertically stretched sheet, *Numer. Heat Transf. Part Appl.*, vol. 0, no. 0, pp. 1–24, doi: 10.1080/10407782.2024.2389338.

20. A. Ahmadi Azar, P. Jalili, B. Jalili and D. D. Ganji, The comprehensive analysis of magnetohydrodynamic Casson fluid flow with rectangular porous medium through expanding/contracting channel, *Multidiscip. Model. Mater. Struct.*, vol. 21, no. 1, pp. 68–97, Oct. 2024, doi: 10.1108/MMMS-07-2024-0179.

21. M. Keimanesh, M. M. Rashidi, A. J. Chamkha and R. Jafari, Study of a third grade non-Newtonian fluid flow between two parallel plates using the multi-step differential transform method, *Comput. Math. Appl.*, vol. 62, no. 8, pp. 2871–2891, Oct. 2011, doi: 10.1016/j.camwa.2011.07.054.

22. S. Team, Reduced Differential Transform Method and Its Application on Kawahara Equations: Reza Abazari, Babak Soltanalizadeh, *Thai J. Math.*, vol. 11, no. 1, Art. no. 1, Apr. 2013.

23. M. Hatami, J. Hatami, M. Jafaryar and G. Domairry, Differential transformation method for Newtonian and Non-Newtonian fluids flow analysis: comparison with HPM and numerical solution, *J. Braz. Soc. Mech. Sci. Eng.*, vol. 38, no. 2, pp. 589–599, Feb. 2016, doi: 10.1007/s40430-014-0275-3.

24. A. Mirzaaghaian and D. D. Ganji, Application of differential transformation method in micropolar fluid flow and heat transfer through permeable walls, *Alex. Eng. J.*, vol. 55, no. 3, pp. 2183–2191, Sep. 2016, doi: 10.1016/j.aej.2016.06.011.

25. P. M. N., N. S. K. and K. Vajravelu, Darcy-Forchheimer nanofluid flow and heat transfer with convective boundary conditions: Insights from differential transform method, *Numer. Heat Transf. Part Appl.*, vol. 86, no. 13, pp. 4374–4400, Jul. 2025, doi: 10.1080/10407782.2024.2318009.

26. U. Khan, I. Waini, A. Zaib, A. Ishak and I. Pop, MHD Mixed Convection Hybrid Nanofluids Flow over a Permeable Moving Inclined Flat Plate in the Presence of Thermophoretic and Radiative Heat Flux Effects, *Mathematics*, vol. 10, no. 7, Art. no. 7, Jan. 2022, doi: 10.3390/math10071164.

27. A. Nayan and N. H. Z. Aznam, Aligned Magnetohydrodynamics (MHD) Flow of Hybrid Nanofluid Over a Vertical Plate Through Porous Medium, vol. 92, no. 1, 2022.

28. B. Venkateswarlu and P. V. Satya Narayana, Cu-Al2O3/H2O hybrid nanofluid flow past a porous stretching sheet due to temperatue-dependent viscosity and viscous dissipation, *Heat Transf.*, vol. 50, no. 1, pp. 432–449, 2021, doi: 10.1002/htj.21884.

29. L. Ebiwareme and K. W. Bunonyo, MHD Fluid Flowing through a Vertical Porous Plate with the Influence of a Magnetic Field and an Angle of Inclination Using the Method of Reduced Differential Transformation, *Asian J. Pure Appl. Math.*, pp. 179–193, Jun. 2023.

30. S. Ahmad, A. M. Rohni and I. Pop, Blasius and Sakiadis problems in nanofluids, *Acta Mech.*, vol. 218, no. 3, pp. 195–204, May 2011, doi: 10.1007/s00707-010-0414-6.

Konduru Sarada,
Department of Mathematics, Government City College,
Nayapul, Hyderabad 500 002, India.
E-mail address: siddisarada@gmail.com

and

J. Komathi,
Post Graduate and Research Department of Mathematics,
Government Arts College for Men,
Krishnagiri 635 001, Tamil Nadu, India.
E-mail address: yazhumathi@gmail.com

and

N. Magesh,
Post Graduate and Research Department of Mathematics,
Government Arts College for Men,
Krishnagiri 635 001, Tamil Nadu, India.
E-mail address: nmagi_2000@yahoo.co.in

and

P. Siva Kota Reddy (Corresponding author),

Department of Mathematics
JSS Science and Technology University
Mysuru-570 006, India.

&

Universidad Bernardo O'Higgins,
Facultad de Ingeniería, Ciencia y Tecnología
Departamento de Formación y Desarrollo Científico en Ingeniería
Av. Viel 1497, Santiago, Chile.
E-mail address: pskreddy@jssstuniv.in

and

Radha Gupta,
Department of Mathematics, HPPC Government First Grade College,
Challakere 577 522, Karnataka, India.
E-mail address: radha.gaurav.gupta@gmail.com

and

C. G. Jagannatha,
Department of Studies in Mathematics, Davangere University,
Davangere 577 007, Karnataka, India.
E-mail address: cgjagannath@gmail.com